

Detailed discussion of discrepancy between theoretical and observed spectral lines in Kr-like W^{38+} based on advanced consideration of core electron correlations

Guo-Qing Peng(彭国庆), Kai Wang(王凯), Jun Yan(颜君), and Wei Kang(康炜)

Citation: Chin. Phys. B, 2025, 34 (**5**): 053101. DOI: 10.1088/1674-1056/adbdbe
Journal homepage: http://cpb.iphy.ac.cn; http://iopscience.iop.org/cpb

What follows is a list of articles you may be interested in

Energy levels and magnetic dipole transition parameters for the nitrogen isoelectronic sequence

Mu-Hong Hu(胡木宏), Nan Wang(王楠), Pin-Jun Ouyang(欧阳品均),Xin-Jie Feng(冯新杰), Yang Yang(杨扬), and Chen-Sheng Wu(武晨晟)
Chin. Phys. B, 2022, 31 (**9**): 093101. DOI: 10.1088/1674-1056/ac7a12

M1 transition energy and rate in the ground configuration of Ag-like ions with $62 \le Z \le 94$

Ju Meng(孟举), Wen-Xian Li(李文显), Ji-Guang Li(李冀光), Ze-Qing Wu(吴泽清), Jun Yan(颜君), Yong Wu(吴勇), and Jian-Guo Wang(王建国)
Chin. Phys. B, 2022, 31 (**1**): 013101. DOI: 10.1088/1674-1056/ac1333

Theoretical study of the hyperfine interaction constants, Landé *g*-factors, and electric quadrupole moments for the low-lying states of the $^{61}Ni^{q+}$ (q=11, 12, 14 , and 15) ions

Ting-Xian Zhang(张婷贤), Yong-Hui Zhang(张永慧), Cheng-Bin Li(李承斌), and Ting-Yun Shi(史庭云)
Chin. Phys. B, 2021, 30 (**1**): 013101. DOI: 10.1088/1674-1056/abc7a3

Effects of electron correlation and the Breit interaction on one- and two-electron one-photon transitions in double K hole states of He-like ions ($10 \le Z \le 47$)

Xiaobin Ding(丁晓彬), Cunqiang Wu(吴存强), Mingxin Cao(曹铭欣), Denghong Zhang(张登红), Mingwu Zhang(张明武), Yingli Xue(薛迎利), Deyang Yu(于得洋), Chenzhong Dong(董晨钟)
Chin. Phys. B, 2020, 29 (**3**): 033101. DOI: 10.1088/1674-1056/ab6c51

Forbidden transition properties of fine-structure $2p^3\,^4S_{3/2}$-$2p^3\,^2D_{3/2,5/2}$ for nitrogen-like ions

Xiao-Kang He(何晓康), Jian-Peng Liu(刘建鹏), Xiang Zhang(张祥), Yong Shen(沈咏), Hong-Xin Zou(邹宏新)
Chin. Phys. B, 2018, 27 (**8**): 083102. DOI: 10.1088/1674-1056/27/8/083102

Detailed discussion of discrepancy between theoretical and observed spectral lines in Kr-like W^{38+} based on advanced consideration of core electron correlations

Guo-Qing Peng(彭国庆)[1], Kai Wang(王凯)[2], Jun Yan(颜君)[1,3,†], and Wei Kang(康炜)[1]

[1] *Center for Applied Physics and Technology, Peking University, Beijing* 100871, *China*
[2] *Department of Physics and Anhui Key Laboratory of Optoelectric Materials Science and Technology, Key Laboratory of Functional Molecular Solids, Ministry of Education, Anhui Normal University, Wuhu* 241000, *China*
[3] *Institute of Applied Physics and Computational Mathematics, Beijing* 100088, *China*

(Received 2 January 2025; revised manuscript received 21 February 2025; accepted manuscript online 7 March 2025)

For the observed line at 799.23 Å in tungsten EBIT experiment, which was assigned to be $^3F_4^o - {}^3F_3^o$ ($[Ar]4s^24p^54d$) of W^{38+} ion, there were noticeable deviations for most calculated wavelengths from the measured value. To clarify this issue, we carry out an extensive calculation for energy levels and transition properties of W^{38+} ion using the multi-configuration Dirac–Hartree–Fock and relativistic configuration interaction method, in which more deeper inner core electron correlations are included, and different forms of Breit interaction as well as quantum electrodynamics corrections are investigated. It is found that the inner core electron correlations can affect the total energy of levels, while only slightly modify the excited energy of levels in $4s^24p^54d$ complex. The present calculated wavelengths agree with the corresponding measured values excellently except the line at 799.23 Å. Thus we are strongly suspicious this line should be misidentified, and suggest that new experiment with higher resolution and spectra analysis based on more accurate atomic data should be performed for W^{38+} ion.

Keywords: Kr-like W^{38+}, the multi-configuration Dirac–Hartree–Fock (MCDHF) method, electron correlation imbalance, Breit interaction, quantum electrodynamic (QED)

PACS: 31.15.vj, 31.15.am, 31.15.xp, 32.70.Cs

DOI: 10.1088/1674-1056/adbdbe **CSTR:** 32038.14.CPB.adbdbe

1. Introduction

When it comes to using magnetic confinement fusion technology for energy application, getting a sustainable and controllable nuclear fusion reaction is of utmost importance. The integration of tungsten as a main material in the critical components, such as the plasma-facing components and divertor, markedly augments system durability and overall performance.[1–5] Thus, this has prompted a worldwide experimental efforts across diverse setups, aimed at assessing the capability of tungsten and accumulating a wealth of experimental data.[6–13]

Typically, these experiments are characterized by temperature ranges in the order of a few keV,[14–19] rendering N-shell tungsten ions prominent contributors to radiation losses. If the tungsten concentration in plasma exceeds acceptable thresholds, intense radiation can cause abrupt quenching of the thermonuclear reaction.[20] Spectroscopic analysis serves as a flexible way to obtain the distribution of ion states, electron density and temperature in the plasma, forming the backbone of evaluating radiation losses.[21–25] Nonetheless, the accurate interpretation of spectrum is inherently dependent on reliable atomic structure calculations.

Moreover, these investigations reciprocally enrich atomic structure theory, deepening our comprehension of multi-electron systems, relativistic and quantum electrodynamic (QED) effects.[26,27] Taking things a step further, incorporating extreme high-density and high-temperature conditions into atomic structure calculations also enables insights into the conditions of astrophysical objects, such as white dwarfs.[28,29] Additionally, atomic structure theory can serve as a cornerstone for testing the standard model (SM) and its extensions.[30–36]

In recent work, there is a noticeable discrepancy between the calculated and measured wavelength (799.23 Å[37]) for $^3F_4^o - {}^3F_3^o$ ($[Ar]4s^24p^54d$) transition of W^{38+}. These calculations have treated 1s, 2s, 2p, 3s, 3p, 3d as core orbitals and 4s, 4p, 4d as valence orbitals to account for different electron correlation effects represented by configuration state functions (CSFs). Among them, Gaigalas *et al.*[38] characterized the atomic state function (ASF) using CSFs, given by $4s^a4p^b4d^cn_1l_1^dn_2l_2^e$, where $a+b+c=6$–8; $d+e=2$–0 and $4 \le n \le 7$; $0 \le l \le (n-1)$ (exclude core orbitals, valence-valence correlation, single-reference (SR) model based solely on the $4s^24p^54d$), with quantum electrodynamics and Breit effects included in their relativistic configuration interaction

†Corresponding author. E-mail: yan_jun@iapcm.ac.cn

© 2025 Chinese Physical Society and IOP Publishing Ltd. All rights, including for text and data mining, AI training, and similar technologies, are reserved.

(RCI) calculations, obtaining a result of 779.46 Å.

Building on the work of Gaigalas *et al.*,[38] Guo *et al.*[39] considered the $3p^5 3d^{10} 4s^a 4p^b 4d^c n_1 l_1^d n_2 l_2^e$ and $3p^6 3d^9 4s^a 4p^b 4d^c n_1 l_1^d n_2 l_2^e$ with $a+b+c=7,8$; $d+e=2,1$ but without 7h, 7i (involve single excitation of the core orbitals 3p and 3d, core–valence correlations), yielding a result of 778.85 Å. Their many-body perturbation (MBPT[40]) method produced a result of 773.24 Å. Sharma *et al.*[41] extended calculations up to $n=8$ but only accounted for core–valence correlations in the 3d orbital, obtaining 789.32 Å (GRASP[42]) and 783.55 Å (FAC[43]). While their value was relatively closer to the measured data, for the $^3D_3^o - {}^3F_3^o$ transition, their computed deviations surpassed Gaigalas *et al.*[38] and roughly ten times larger than those of Guo *et al.*[39] Hence, more in-depth theoretical and experimental research is warranted.

In theory, accurately describing the Hamiltonian of a multi-electron atom and expanding its wave function with an infinite series of single-electron function product would allow precise calculation of any physical properties. Practically though, approximations and truncations are necessary.[38,39,41] And in the process of truncation, it is inevitable to encounter the different order of wave function retention for various energy levels, and even the retention of the same order is not fully included, which induce the electron correlation imbalance.

This paper aims to refine existing approximation methods, elevate the truncation threshold and look forward to a plausible explanation that could shed some light on this discrepancy. To this end, a systematically computational study is undertaken for energies and transition properties for all energy levels of the $4p^6$ and $4p^5 4d$ in W^{38+}. Our calculation extensively explored single and double electron excitations down to the 2s subshell. It also included higher excitations of core orbitals and multireference to address electron correlation imbalances due to core–core correlations, which were observed through changes in both absolute energy and radial electron density distribution. Besides, we incorporated Breit corrections beyond the low-frequency limit, and accounted for self-energy in QED with methods including finite nuclear size effects and enhanced screening,[44–46] as well as the non-local components.[47,48] Breit and QED are calculated within RCI.

2. Theoretical method

2.1. MCDHF

Calculations in this paper were carried out utilizing the multi-configuration Dirac–Hartree–Fock (MCDHF)[42,49] method provided by GRASP,[50] since this method has already achieved a number of reliable results in calculating atomic properties.[38,39,41,51–53] In the MCDHF method, the ASF Ψ is a linear combination of CSFs Φ

$$\Psi(\Gamma PJ) = \sum_{i=1}^{N} c_i \Phi(\gamma_i PJ), \tag{1}$$

where P is the parity, J is the total angular momentum, γ_i is chosen to uniquely define the CSF, Γ is usually the same with the γ_i of the dominant CSF component, and c_i is the i-th component of the eigenvector for the Hamiltonian (3) matrix elements based on CSFs. The CSF is constructed by coupling the angular momentum and antisymmetrizing single-electron Dirac function $u(\boldsymbol{r})$ product

$$u(\boldsymbol{r}) = \frac{1}{r}\begin{pmatrix} P_{n\kappa}(r)\chi_{\kappa m}(\theta,\phi) \\ \mathrm{i}Q_{n\kappa}(r)\chi_{-\kappa m}(\theta,\phi) \end{pmatrix}, \tag{2}$$

where χ are the spinor spherical harmonics. The radial large (P) and small (Q) component are obtained by applying the variational principle on the energy functional of the targeted states in the extended optimal level (EOL) scheme, and their convergence is established by means of the self-consistent field process (SCF).[42,49] The energy functional is based on the Dirac–Coulomb Hamiltonian (in units of a.u.)

$$H = \sum_{i=1}^{N}\left[c\boldsymbol{\alpha}_i\boldsymbol{p}_i + (\beta_i - 1)c^2 + V(r_i)\right] + \sum_{1=i<j}^{N}\frac{1}{r_{ij}}, \tag{3}$$

where $\boldsymbol{\alpha}$ and β are 4×4 Dirac matrices, $\boldsymbol{p}$ is the momentum operator, $V(r_i)$ and $1/r_{ij}$ are the electrostatic electron–nucleus and electron–electron interactions, respectively.

The CSFs, as the starting point to fabricate the Hamiltonian (3) matrix elements, can be generated by allowing singe and double excitations of the targeted states to a set of orbitals. For capturing higher-order effects accurately, triple and quadrupole excitations are also required. However, in complex ion systems like W, the rapid increase in the number of CSFs renders the computation prohibitively difficult. An alternative strategy, therefore, is adopting the multireference (MR) method, which effectively accounts for higher-order corrections by including single and double excitations from strongly interacting configurations with the target state.[27,54–56]

2.2. Breit and QED

We took into account the Breit interaction and QED corrections in the final relativistic configuration-interaction (RCI) calculations.

Except for the Coulomb interaction ($1/r_{ij}$), the electron–electron interaction due to one-photon exchange also includes the transverse photon (TP) interaction,[57,58] and can be written in the Coulomb gauge as

$$\begin{aligned} H_{\mathrm{TP}} = -\sum_{1=i<j}^{N}\Bigg[&\frac{\boldsymbol{\alpha}_i\cdot\boldsymbol{\alpha}_j}{r_{ij}} + \frac{\boldsymbol{\alpha}_i\cdot\boldsymbol{\alpha}_j}{r_{ij}}\left(\cos(\omega_{ij}r_{ij}/c) - 1\right) \\ &- (\boldsymbol{\alpha}_i\cdot\boldsymbol{\nabla}_i)(\boldsymbol{\alpha}_j\cdot\boldsymbol{\nabla}_j)\frac{\cos(\omega_{ij}r_{ij}/c) - 1}{\omega_{ij}^2 r_{ij}/c^2}\Bigg], \end{aligned} \tag{4}$$

where ω_{ij} is the frequency of the exchanged virtual photon between the two electrons, $\boldsymbol{\nabla}$ operator acts on the r_{ij} but not on the following wave functions. In Eq. (4), the first term is

magnetic interaction and the last two terms containing ω_{ij} represent the retardation interaction. When $\omega_{ij} \to 0$, the TP interaction reduces to the Breit interaction[59]

$$H_{\text{Briet}} = -\sum_{1=i<j}^{N} \frac{1}{2r_{ij}} \left[\boldsymbol{\alpha}_i \cdot \boldsymbol{\alpha}_j + \frac{(\boldsymbol{\alpha}_i \cdot \boldsymbol{r}_{ij})(\boldsymbol{\alpha}_j \cdot \boldsymbol{r}_{ij})}{r_{ij}^2} \right]. \quad (5)$$

The QED features two main radiative correction types: self-energy (SE) and vacuum polarization (VP). The one-loop VP can be expressed in terms of a potential consisting of the Uehling potential (of order $Z\alpha$)[60] and the Wichmann and Kroll potential (of order $(Z\alpha)^3$ and higher).[61] And the two-loop VP can be calculated using the Källén–Sabry potential.[62,63] There is no concise algorithm for one and more loops SE, but the correction (ΔE_{SE}) can be formalized as

$$\Delta E_{\text{SE}} = \left(\frac{\alpha}{\pi}\right) \frac{\alpha^2 Z^4}{n^3} F(nlj, Z\alpha), \quad (6)$$

where $F(nlj, Z\alpha)$ is retrieved from the tabulated data provided by Mohr,[64] Klarsfeld and Maquet,[65] based on the parameters Z, n, l, and j. Given the slow variation of $F(nlj, Z\alpha)$ with respect to $Z\alpha$, interpolated values can be suitably derived for Z not listed in the table. Up to this point, there have been roughly three methods to improve or extend Eq. (6).

(i) SE1: employing a screened hydrogenic approximation by multiplying the ratio of the mean radius for MCDHF orbitals to that of hydrogenic orbitals.

(ii) SE2: incorporating finite-nuclear size effects for the hydrogenic values,[44,45] with the screening approximation improved through the Welton interpretation – this involves multiplying the ratio of the mean value of $\Delta V(x)$ associated with MCDHF orbitals relative to hydrogenic ones.[46]

(iii) SE3: utilizing the model-QED operator developed by Shabaev *et al.*[47] and Malyshev *et al.*,[48] which involves a nonlocal QED component to calculate SE corrections.

3. Results and discussion

3.1. Electron correlation

We adopted a method for constructing CSFs similar to those outlined in Section 1,[38,39,41] but tailored to capture extensive electron correlations involving deeper orbitals and MR. Our model defined $1s^2$ as the inactive core, while $2s^22p^63s^23p^63d^{10}$ as the active core, with $4s^24p^6$ and $4s^24p^54d$ serving as active valence for even and odd parities, respectively, and optimized them separately and independently. Given the complexities related to convergence, we confined SCF optimization of the radial wave functions to valence–valence correlation, then generated the CSFs of core–valence and core–core correlations using these wave functions. As convergence is approached, the trends in energy between different energy levels become similar across different correlations. Figure 1 only displays a representative subset, that is, the energy levels ($^3F_3^o$, $^3F_4^o$) originally assigned by the spectral line 799.23 Å and the energy level ($^1P_1^o$) converging from the opposite direction of the valence–valence correlation.

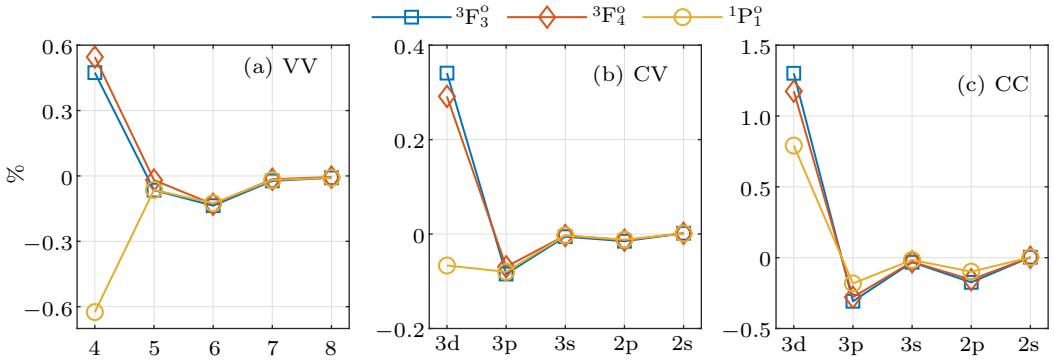


Fig. 1. Convergence of the excited energy (relative to the ground state $4p^6$) for levels $^3F_3^o$ (squares), $^3F_4^o$ (diamonds), and $^1P_1^o$ (circles). The level of convergence is characterized by the relative change in energy ($E_{\text{latter}}/E_{\text{former}} - 1$). (a) Valence–valence correlation (VV) with the principal quantum number n; (b) core–valence correlation (CV); (c) core–core correlation (CC), both panels (b) and (c) with subshell nl (l is orbital angular momentum).

(i) Valence–valence correlation (VV): we included single and double excitations from the valence orbitals to the sets with $4 \le n \le 8$ and $0 \le l \le (n-1)$ (with each successive layer outward, i.e., $n = 5$ indicates that a shell with a principal quantum number of 5 is added on the basis of $n = 4$). Figure 1(a) shows convergence of energy levels at $n = 8$ from both positive and negative directions, with the relative change in excited energy ($E_{\text{latter}}/E_{\text{former}} - 1$) not exceeding 0.01%.

(ii) Core–valence correlation (CV): building on the VV correlation to $n = 8$, we considered single excitation of one electron from core (with each successive layer inward, i.e., 3p indicates that the subshells 3p and 3d are opened, same for core–core correlation) and at most one electron from valence orbitals up to $n = 6$ and $0 \le l \le (n-1)$. Figure 1(b) indicates converging at the 2p subshell opening, with the relative change remaining below 0.002%. Additionally, we observed that the order of the $^1P_1^o$ had altered as indicated in Guo *et al.*[39]

(iii) Core–core correlation (CC): based on the CV correlation to 2p, we employed double excitations of electrons from the core orbitals up to $n = 6$ and $0 \le l \le (n-1)$. Figure 1(c)

demonstrates energy level convergence upon reaching the 2p subshell, with a relative change of 0.003%.

In analyzing the three subplots within Fig. 1, a remarkable deviation in the initial point is noticeable for the CC compared to the other two. Prompted by it, we analyzed the variation in radial electron density[56,66] ($D(r) = 4\pi r^2\rho(r)$), which represents the total electron density, including all core and valence electrons, and was calculated through the program rdensity[50] in GRASP. The difference in radial electron density of the electron correlation model under different parity of $J = 0$ (mirror for other J-values) corresponding to the starting points in Fig. 1(b) (CV to 3d and VV to $n = 8$) and Fig. 1(c) (CC to 3d and CV to 2p), as illustrated in Figs. 2(a) and 2(b), with the sub-titles "cv_3d-vv_8" and "cc_3d-cv_2p", show the overall distribution of the electron cloud expands into the outer space upon the excitation of core electrons. The yellow dotted line in Fig. 2(a) presents the distribution of the radial electron density (multiplied by 10^{-4}) of the even parity $4p^6$ under VV to $n = 8$ as a background reference, with almost no significant differences in the distribution under odd parity or other electron correlations. Intuitively, the closed-shell $4p^6$ in even parity, which, due to its compact nature, facilitates stronger core–valence electron exchange interactions and thereby easier to pull the core electrons towards the valence shells compared to the more diffuse $4p^5 4d$ in odd parity,[55,56] but the situation depicted in Fig. 2(b), suggests the opposite. Meanwhile, we found that the decrease in absolute energy for even parity was notably greater than that for odd parity when CC is considered. Further exploration involved exciting at least one electron to $n = 7$ and $0 \le l \le (n-1)$ from 3p and 3d based on CC to 2p for both parities, leading to radial electron density difference in Fig. 2(c), with the sub-title "ccv_3p_7-cc_2p", indicating a more prominent electron density contraction for odd parity relative to even parity. And this also led to the absolute energy reduction becoming marginally more pronounced for the odd parity. These all indicate an imbalance in the electronic correlation between odd and even parities under these conditions.

In pursuit of better electron correlation balance by considering higher-order electron correlation effects through MR, we assessed the MR $\{4p^4 4d^2, 4p^4 4f^2\}$ for even parity, which shows nearly matching energy shifts for odd and even parities, and induces a weak modification of the even-parity radial electronic density, as is visible in Fig. 2(d), with the sub-title "even_mr-ccv_3p_7". Due to computational limitations, we ultimately incorporated $\{4s4p^5 4d^2\}$ $\{4p^5 5p, 4s5s, 4s4p^5 5s5p, 4p^4 5p^2, 3s5s, 3p^5 5p\}$ as additional multireferences for odd and even parities, respectively, onto the preceding CSFs. Overall, if the electron correlation is unbalanced, the excited energy of the odd parity levels, referenced to the ground state even parity energy, becomes unreliable, and the electron density, as shown in Figs. 2(b) and 2(c), is also distorted. However, after properly addressing the electronic correlation imbalance, the correction to the excited energy is approximately 0.2 eV, while the correction to the absolute energy of the odd and even parity levels is more than 8 eV, two orders of magnitude larger than the former. At this point, the calculated wavelength for $^3F_4^o - {}^3F_3^o$ transition is 758.71 Å, considerably less than the measured 799.23 Å, necessitating further theoretical modification.

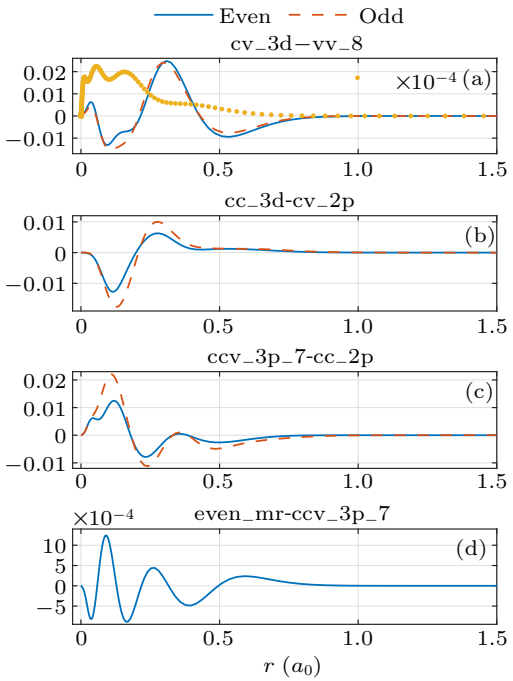


Fig. 2. Radial electron density difference associated with different electron correlation models for two levels, i.e., even parity $4p^6$ (blue solid line) and odd parity $4p^5 4d$ (red dashed line) at $J = 0$. The yellow dotted line in (a) displays the distribution of the radial electron density (multiplied by 10^{-4}) of the even parity $4p^6$ under VV to $n = 8$. The hyphen-separated subtitle above each subplot suggests the radial electron density difference of the two (left and right of the hyphen) electron correlation models. See the text for details.

3.2. Impact of Breit and QED corrections

The transition wavelength for $^3F_4^o$–$^3F_3^o$, calculated without including Breit and QED corrections in RCI, is significantly lower than the measured value. Therefore, following the final proposal in the Subsection 3.1, an evaluation was undertaken to examine the influences of Breit and QED on the excited energy. To facilitate comparisons with other research, we have provided both jj-coupled and LSJ-coupled labels and applied the jj-LSJ transformation method[67] to convert jj-coupled CSFs into LSJ-coupled CSFs. As Table 1 reveals, the Breit interaction exerts an arresting effect on excited energy, with a range spanning roughly from -15500 cm^{-1} to -2500 cm^{-1}. And the frequency-dependent effect (4) can modulate the strength of Breit by -40% to 2%. Although substituting the Breit (Eq. (5)) with TP (Eq. (4)) for the targeted energy levels ($^3F_4^o$, $^3F_3^o$) introduces a uniform directional shift of nearly equal in magnitude, TP was preferred in our calcu-

lations due to its potential to facilitate the future identification of additional spectral lines.

Table 1 also indicates the effect of QED on excited energy ranging from -1650 cm^{-1} to -500 cm^{-1}, weaker than Breit. Meanwhile, Table 2 presents a slightly improved agreement between the SE2 model with the measured values, as this advantage remains statistically inconclusive. However, the calculation results of other systems (W^{56+}–W^{61+}) by Zhang *et al.*[51,52] show the superiority of SE2 and SE3 over SE1. For the system under our study, the approximations arising from the selection of the nuclear model and screening in SE2,[44–46] along with that from the restricting matrix elements to low-lying wave functions in SE3,[47,48] cannot be overshadowed by the progress made in considering more physical effects in both methods. These complexities highlight the need for comprehensive, case-specific benchmarking studies to evaluate the accuracy and predictive power of SE2 and SE3. Currently, the computed wavelength (777.03 Å) remains significantly lower than the experimental measurement value of 799.23 Å.

Table 1. Contributions of Breit and QED corrections to the excited energy (relative to the ground state $4p^6$, in unit cm^{-1}). DC represents the excited energy without Breit and QED corrections. Breit and TP refer to the calculations using Eqs. (5) and (4), respectively. $\Delta_{\rm Breit} = E_{\rm TP} - E_{\rm Breit}$. SE1–SE3 correspond to the three different methods mentioned in Subsection 2.2 for calculating self-energy (see the text for details), representing the combined contributions of self-energy and vacuum polarization to the excited energy.

Key	LS	jj	DC	Breit	TP	$\Delta_{\rm Breit}$	SE1	SE2	SE3
1	$4p^5 4d\ ^3P^o_0$	$(\frac{3}{2},\frac{3}{2})_0$	1208416	–3586	–2568	1018	–1507	–1624	–1512
2	$4p^5 4d\ ^3P^o_1$	$(\frac{3}{2},\frac{3}{2})_1$	1244833	–4256	–3245	1011	–1490	–1598	–1496
3	$4p^5 4d\ ^3F^o_3$	$(\frac{3}{2},\frac{3}{2})_3$	1270036	–4492	–3472	1020	–1504	–1621	–1510
4	$4p^5 4d\ ^3D^o_2$	$(\frac{3}{2},\frac{3}{2})_2$	1278648	–4112	–3094	1018	–1505	–1621	–1511
5	$4p^5 4d\ ^3F^o_4$	$(\frac{3}{2},\frac{5}{2})_4$	1401839	–7862	–6954	908	–1264	–1247	–1273
6	$4p^5 4d\ ^1D^o_2$	$(\frac{3}{2},\frac{5}{2})_2$	1416499	–7451	–6546	905	–1270	–1254	–1280
7	$4p^5 4d\ ^3D^o_3$	$(\frac{3}{2},\frac{5}{2})_3$	1460506	–7476	–6565	911	–1270	–1254	–1280
8	$4p^5 4d\ ^3D^o_1$	$(\frac{3}{2},\frac{5}{2})_1$	1574585	–7521	–6652	869	–1256	–1259	–1277
9	$4p^5 4d\ ^3F^o_2$	$(\frac{1}{2},\frac{3}{2})_2$	1999606	–11826	–11987	–161	–740	–894	–913
10	$4p^5 4d\ ^1P^o_1$	$(\frac{1}{2},\frac{3}{2})_1$	2157825	–11606	–11698	–92	–776	–921	–940
11	$4p^5 4d\ ^3P^o_2$	$(\frac{1}{2},\frac{5}{2})_2$	2161150	–14639	–14909	–270	–508	–528	–685
12	$4p^5 4d\ ^1F^o_3$	$(\frac{1}{2},\frac{5}{2})_3$	2183318	–15168	–15441	–273	–505	–525	–682

Table 2. Comparisons of transition wavelengths (in unit Å) between TP+QED using various self-energy models (SE1–SE3, mentioned in Subsection 2.2, see the text for details) and experimental data in NIST. $\Delta\lambda/\lambda = (\lambda_{\rm theory} - \lambda_{\rm exp})/\lambda_{\rm exp}$ (%).

	λ				$\Delta\lambda/\lambda$		
Type	Exp	TP+SE1	TP+SE2	TP+SE3	TP+SE1	TP+SE2	TP+SE3
M1	532.87	533.02	532.64	533.03	0.0274	–0.0435	0.0296
	559.04	559.84	559.43	559.85	0.1435	0.0694	0.1458
	799.23	777.84	777.03	777.86	–2.6768	–2.7775	–2.6736
E1	80.64	80.639	80.646	80.639	–0.0015	0.0072	–0.0010
	63.883	63.829	63.829	63.830	–0.0840	–0.0838	–0.0826
	46.67	46.612	46.616	46.616	–0.1233	–0.1166	–0.1157

3.3. Discrepancy analysis

As discussed above, by incorporating CC, MR, TP, and SE2 in the QED correction, the calculated $^3F^o_4 - ^3F^o_3$ transition wavelength is 777.03 Å. After accounting for CC and MR, it differs by only ones place from the value obtained with CV and SR. Meanwhile, the impact of varying Breit and self-energy models is limited to the first decimal place. Compared to the measured value of 799.23 Å, the relative deviation is -2.8%, which is one or two orders of magnitude larger than the relative deviations of other spectral lines, as evidenced in Table 2. This resonates with Gaigalas *et al.*[38] and Guo *et al.*,[39] but contrasts with Sharma *et al.*[41] Similarly, for W^{39+} spectral line with an measured value of 774.8 Å, as the computational accuracy increases, the relative deviation between the measured and calculated value for this line shows little improvement.[68,69]

The experimental data for the aforementioned two spectral lines were sourced from the Electron Beam Ion Trap (EBIT) experiment performed by Radtke.[37] Within this experiment, the electron energy spread was comparable to the ionization energy difference between W^{38+} and W^{39+}, and the absolute intensity of spectral lines was susceptible to disturbance. Thus, we suspect that the 774.8 Å line corresponds to the experimental value of $^3F^o_4 - ^3F^o_3$, considering its reduced deviation – merely a few tenths of a percent – from the majority of theoretical calculations. The conclusion drawn without conducting collision radiation simulations, is based on the following rationale: previous works have established that $^3F^o_4 - ^3F^o_3$ transition is strong, and in the original experiment, two resolvable spectral lines were observed at 799.32 Å and

774.8 Å, and based on the current calculations, it may be more appropriate to consider 774.8 Å as the experimental value for $^3F^o_4$–$^3F^o_3$. Certainly, this requires further collision radiation simulations for different ionization states, based on high-precision calculations, as well as experimental validation. Under this adjustment, the energy of $^3F^o_4$ in NIST requires rectification, rather than $^3F^o_3$, because the energy of $^3D^o_3$ (derived from the energy of $^3F^o_3$ and the wavelength of $^3D^o_3 - {}^3F^o_3$) aligns well with our results and those in Gaigalas *et al.*[38] and Guo *et al.*[39] Subsequent implications coming from the spectral reassignment of this transition can be inferred from the data furnished in Tables 3 and 4.

Table 3. Excited energies (relative to the ground state $4p^6$, in unit cm^{-1}) for levels $4p^6$ and $4p^54d$ of W^{38+} from our calculation (TP+SE2, E_{our}) and previous data. E_{NIST}[70] (5^a was adjusted according to 774.8 Å.); E_{98};[71] E_{15};[38] E^a_{16},[39] (MCDHF); E^b_{16}[39] (RMBPT); E^a_{19}[41] (GRASP); E^b_{19}[41] (FAC).

Key	LS	jj	E_{NIST}	E_{98}	E_{15}	E^a_{16}	E^b_{16}	E^a_{19}	E^b_{19}	E_{our}
0	$4p^6\ ^1S^e_0$	$(0,0)_0$	0	0	0	0	0	0	0	0
1	$4p^54d\ ^3P^o_0$	$(\frac{3}{2},\frac{3}{2})_0$	1208000	1198704	1203118	1203570	1205201	1199868	1201294	1204225
2	$4p^54d\ ^3P^o_1$	$(\frac{3}{2},\frac{3}{2})_1$	1240000	1236314	1239448	1239427	1240953	1237157	1238386	1239990
3	$4p^54d\ ^3F^o_3$	$(\frac{3}{2},\frac{3}{2})_3$	1264000	1261312	1264594	1264782	1265721	1264130	1264942	1264943
4	$4p^54d\ ^3D^o_2$	$(\frac{3}{2},\frac{3}{2})_2$	1272800	1272663	1273846	1273588	1274670	1273995	1274818	1273933
5	$4p^54d\ ^3F^o_4$	$(\frac{3}{2},\frac{5}{2})_4$	1389120							
5^a	$4p^54d\ ^3F^o_4$	$(\frac{3}{2},\frac{5}{2})_4$	1393066	1386631	1392887	1393177	1395047	1390822	1392567	1393638
6	$4p^54d\ ^1D^o_2$	$(\frac{3}{2},\frac{5}{2})_2$	1409000	1407083	1408445	1408207	1409714	1406832	1408478	1408699
7	$4p^54d\ ^3D^o_3$	$(\frac{3}{2},\frac{5}{2})_3$	1451660	1452370	1452685	1452487	1453759	1452856	1454019	1452687
8	$4p^54d\ ^3D^o_1$	$(\frac{3}{2},\frac{5}{2})_1$	1565350	1579125	1571375	1566184	1561730	1581841	1582083	1566674
9	$4p^54d\ ^3F^o_2$	$(\frac{1}{2},\frac{3}{2})_2$		1985853	1985683	1987261	1986787	1986070	1989537	1986724
10	$4p^54d\ ^1P^o_1$	$(\frac{1}{2},\frac{3}{2})_1$	2142690	2167239	2152772	2145671	2138019	2167641	2169507	2145205
11	$4p^54d\ ^3P^o_2$	$(\frac{1}{2},\frac{5}{2})_2$			2144754	2146087	2146119	2143993	2147998	2145713
12	$4p^54d\ ^1F^o_3$	$(\frac{1}{2},\frac{5}{2})_3$		2168010	2166530	2168024	2167712	2166269	2170165	2167352

Table 4. Transition data for E1, M1, E2, M2, and E3 from the $4p^6$ and $4p^54d$ (inclusion of transitions with lifetime contributions exceeding 5×10^{-6} only), the transition wavelength λ (in unit Å), transition rate A (in unit s^{-1}, length form), oscillator strength gf (in unit a.u., length form), and line strength S (in unit a.u., length form), S_{15} (in unit a.u., length form),[38] S_{16} (in unit a.u., length form),[39] $\delta S = (S_{velocity} - S_{length})/\max(S_{length}, S_{velocity})$ (%), $\Delta S_{15} = (S_{15} - S)/S$ (%), $\Delta S_{16} = (S_{16} - S)/S$ (%).

Upper	Lower	Type	λ	A	gf	S	S_{15}	S_{16}	δS	ΔS_{15}	ΔS_{16}
2	0	E1	80.646	2.66×10^9	7.77×10^{-3}	2.06×10^{-3}	2.04×10^{-3}	2.05×10^{-3}	3.5	–1.3	–0.7
2	1	M1	2796.0	6.06×10^2	2.13×10^{-6}	1.47×10^0	1.48×10^0	1.47×10^0		0.2	0.1
3	0	E3	79.055	2.12×10^1	1.39×10^{-10}	9.10×10^{-3}		9.07×10^{-3}	–0.1		–0.3
4	0	M2	78.497	8.69×10^1	4.01×10^{-10}	8.69×10^{-2}		8.84×10^{-2}			1.8
4	2	E2	2946.0	2.76×10^{-2}	1.80×10^{-10}	2.74×10^{-2}	2.75×10^{-2}		–1.6	0.42	
4	2	M1	2946.0	3.39×10^2	2.20×10^{-6}	1.61×10^0	1.60×10^0	1.61×10^0		–0.1	0.1
4	3	M1	11122	6.64×10^0	6.16×10^{-7}	1.69×10^0	1.70×10^0	1.70×10^0		0.0	0.2
5	3	E2	777.03	6.42×10^0	5.23×10^{-9}	1.46×10^{-2}	1.47×10^{-2}		1.1	0.4	
5	3	M1	777.03	2.47×10^4	2.01×10^{-5}	3.87×10^0	3.87×10^0	3.87×10^0		0.1	0.1
5	4	E2	835.39	1.02×10^0	9.63×10^{-10}	3.34×10^{-3}	3.34×10^{-3}	3.31×10^{-3}	11	–0.2	–1.0
6	0	M2	70.988	1.39×10^4	5.26×10^{-8}	8.42×10^0		8.43×10^0			0.0
6	1	E2	489.06	2.50×10^1	4.48×10^{-9}	3.12×10^{-3}	3.14×10^{-3}	3.11×10^{-3}	–3.7	0.6	–0.5
6	2	M1	592.74	3.11×10^4	8.20×10^{-6}	1.20×10^0	1.20×10^0	1.20×10^0		–0.0	–0.1
6	3	E2	695.62	2.32×10^0	8.42×10^{-10}	1.69×10^{-3}	1.70×10^{-3}		–3.2	0.4	
6	3	M1	695.62	2.07×10^3	7.50×10^{-7}	1.29×10^{-1}	1.30×10^{-1}	1.30×10^{-1}		0.9	0.5
6	4	E2	742.03	2.96×10^0	1.22×10^{-9}	2.97×10^{-3}	2.97×10^{-3}		–4.3	0.1	
6	4	M1	742.03	1.21×10^4	5.00×10^{-6}	9.18×10^{-1}	9.20×10^{-1}	9.19×10^{-1}		0.3	0.1
7	0	E3	68.838	5.10×10^1	2.53×10^{-10}	8.31×10^{-3}		8.31×10^{-3}	0.1		0.0
7	2	E2	470.15	1.69×10^1	3.92×10^{-9}	2.43×10^{-3}	2.42×10^{-3}	2.41×10^{-3}	–2.1	–0.4	–0.6
7	3	E2	532.64	2.12×10^1	6.30×10^{-9}	5.67×10^{-3}	5.70×10^{-3}		–7.0	0.5	
7	3	M1	532.64	1.55×10^4	4.60×10^{-6}	6.06×10^{-1}	6.06×10^{-1}	6.08×10^{-1}		–0.1	0.3
7	4	E2	559.43	7.48×10^0	2.46×10^{-9}	2.56×10^{-3}	2.59×10^{-3}		–0.3	1.2	
7	4	M1	559.43	4.52×10^4	1.48×10^{-5}	2.05×10^0	2.05×10^0	2.05×10^0		0.0	–0.1
7	5	E2	1693.5	1.02×10^0	3.07×10^{-9}	8.89×10^{-2}	8.95×10^{-2}		–10	0.6	
7	5	M1	1693.5	7.08×10^1	2.13×10^{-7}	8.92×10^{-2}	8.96×10^{-2}	8.79×10^{-2}		0.4	–1.5
7	6	M1	2273.3	2.37×10^1	1.28×10^{-7}	7.22×10^{-2}	7.15×10^{-2}	7.19×10^{-2}		–0.9	–0.4

Table 4. (*Continued*).

Upper	Lower	Type	λ	A	gf	S	S_{15}	S_{16}	δS	ΔS_{15}	ΔS_{16}
8	0	E1	63.829	6.11×10^{11}	1.12×10^{0}	2.35×10^{-1}	2.40×10^{-1}	2.36×10^{-1}	–4.2	1.8	0.1
8	1	M1	275.90	1.51×10^{5}	5.18×10^{-6}	3.53×10^{-1}	3.55×10^{-1}	3.53×10^{-1}		0.6	–0.2
8	2	E2	306.11	2.78×10^{2}	1.17×10^{-8}	2.00×10^{-3}	2.01×10^{-3}		0.4	0.5	
8	2	M1	306.11	2.19×10^{5}	9.22×10^{-6}	6.98×10^{-1}	7.08×10^{-1}	6.97×10^{-1}		1.3	–0.2
8	3	E2	331.42	3.61×10^{2}	1.78×10^{-8}	3.87×10^{-3}	4.15×10^{-3}	3.84×10^{-3}	7.5	7.3	–0.7
8	4	E2	341.60	9.36×10^{2}	4.91×10^{-8}	1.17×10^{-2}	1.20×10^{-2}		–2.6	2.8	
8	4	M1	341.60	1.24×10^{5}	6.49×10^{-6}	5.48×10^{-1}	5.64×10^{-1}	5.48×10^{-1}		2.9	0.0
8	6	E2	633.01	1.07×10^{1}	1.93×10^{-9}	2.91×10^{-3}	2.92×10^{-3}		–9.1	0.2	
8	6	M1	633.01	1.17×10^{3}	2.12×10^{-7}	3.31×10^{-2}	3.30×10^{-2}	3.33×10^{-2}		–0.5	0.4
8	7	E2	877.30	4.84×10^{0}	1.68×10^{-9}	6.74×10^{-3}	6.73×10^{-3}	6.69×10^{-3}	–17	–0.1	–0.7
9	0	M2	50.334	1.79×10^{3}	3.39×10^{-9}	1.93×10^{-1}		1.93×10^{-1}			–0.1
9	1	E2	127.80	4.28×10^{4}	5.24×10^{-7}	6.52×10^{-3}	6.59×10^{-3}	6.49×10^{-3}	–0.9	1.1	–0.4
9	2	E2	133.92	7.95×10^{4}	1.07×10^{-6}	1.53×10^{-2}	1.54×10^{-2}		0.2	0.8	
9	2	M1	133.92	3.22×10^{5}	4.32×10^{-6}	1.43×10^{-1}	1.43×10^{-1}	1.43×10^{-1}		–0.2	–0.0
9	3	E2	138.55	8.34×10^{4}	1.20×10^{-6}	1.90×10^{-2}	1.91×10^{-2}		0.3	0.7	
9	3	M1	138.55	4.72×10^{6}	6.79×10^{-5}	2.33×10^{0}	2.38×10^{0}	2.33×10^{0}		2.3	0.1
9	4	E2	140.29	8.83×10^{4}	1.30×10^{-6}	2.14×10^{-2}	2.16×10^{-2}		–1.1	0.6	
9	4	M1	140.29	1.66×10^{6}	2.44×10^{-5}	8.48×10^{-1}	8.49×10^{-1}	8.48×10^{-1}		0.1	–0.0
9	5	E2	168.61	1.74×10^{1}	3.71×10^{-10}	1.06×10^{-5}	1.07×10^{-5}	1.05×10^{-5}	–14	0.5	–1.3
9	6	E2	173.00	4.68×10^{2}	1.05×10^{-8}	3.24×10^{-4}	3.31×10^{-4}		–2.8	2.1	
9	6	M1	173.00	1.21×10^{4}	2.72×10^{-7}	1.17×10^{-2}	1.18×10^{-2}	1.18×10^{-2}		1.4	1.3
9	7	E2	187.25	1.27×10^{2}	3.34×10^{-9}	1.31×10^{-4}	1.32×10^{-4}		–2.2	1.0	
9	7	M1	187.25	6.70×10^{3}	1.76×10^{-7}	8.15×10^{-3}	8.11×10^{-3}	8.48×10^{-3}		–0.5	4.1
9	8	E2	238.07	9.29×10^{2}	3.95×10^{-8}	3.17×10^{-3}	3.35×10^{-3}		1.6	5.7	
9	8	M1	238.07	1.17×10^{4}	4.95×10^{-7}	2.91×10^{-2}	3.02×10^{-2}	2.92×10^{-2}		3.6	0.0
10	0	E1	46.616	2.08E+12	2.03×10^{0}	3.11×10^{-1}	3.34×10^{-1}	3.11×10^{-1}	–2.3	7.2	–0.1
10	1	M1	106.27	1.21×10^{6}	6.14×10^{-6}	1.61×10^{-1}	1.57×10^{-1}	1.62×10^{-1}		–3.1	0.1
10	2	E2	110.47	1.68×10^{4}	9.24×10^{-8}	7.42×10^{-4}	7.13×10^{-4}		2.9	–3.9	
10	2	M1	110.47	2.87×10^{6}	1.58×10^{-5}	4.31×10^{-1}	4.18×10^{-1}	4.31×10^{-1}		–3.0	0.1
10	3	E2	113.60	4.63×10^{5}	2.69×10^{-6}	2.35×10^{-2}	2.33×10^{-2}	2.33×10^{-2}	–1.3	–0.6	–0.7
10	4	E2	114.78	1.17×10^{5}	6.96×10^{-7}	6.26×10^{-3}	6.11×10^{-3}		0.2	–2.5	
10	4	M1	114.78	3.17×10^{6}	1.88×10^{-5}	5.33×10^{-1}	5.19×10^{-1}	5.33×10^{-1}		–2.5	0.1
10	6	E2	135.78	8.53×10^{1}	7.07×10^{-10}	1.05×10^{-5}	8.50×10^{-6}		8.4	–19	
10	6	M1	135.78	1.45×10^{4}	1.21×10^{-7}	4.05×10^{-3}	3.95×10^{-3}	4.13×10^{-3}		–2.4	2.1
10	7	E2	144.40	3.74×10^{3}	3.51×10^{-8}	6.30×10^{-4}	6.71×10^{-4}	6.34×10^{-4}	–9.1	6.6	0.6
10	8	E2	172.85	8.98×10^{2}	1.21×10^{-8}	3.71×10^{-4}	3.88×10^{-4}		1.8	4.6	
10	8	M1	172.85	1.58×10^{5}	2.12×10^{-6}	9.05×10^{-2}	9.15×10^{-2}	9.07×10^{-2}		1.0	0.2
10	9	E2	630.99	2.77×10^{1}	4.95×10^{-9}	7.41×10^{-3}	7.28×10^{-3}		–8.9	–1.7	
10	9	M1	630.99	1.17×10^{3}	2.09×10^{-7}	3.26×10^{-2}	3.19×10^{-2}	3.27×10^{-2}		–2.3	0.1
11	0	M2	46.605	1.52×10^{4}	2.47×10^{-8}	1.12×10^{0}		1.12×10^{0}			0.0
11	1	E2	106.22	5.56×10^{2}	4.70×10^{-9}	3.35×10^{-5}	3.62×10^{-5}	3.47×10^{-5}	–11	7.9	3.4
11	2	E2	110.41	2.41×10^{2}	2.20×10^{-9}	1.77×10^{-5}	1.74×10^{-5}		9.3	–1.4	
11	2	M1	110.41	1.67×10^{5}	1.52×10^{-6}	4.16×10^{-2}	4.22×10^{-2}	4.17×10^{-2}		1.4	0.3
11	3	E2	113.54	2.86×10^{3}	2.76×10^{-8}	2.41×10^{-4}	2.45×10^{-4}		–7.4	2.0	
11	3	M1	113.54	4.93×10^{3}	4.76×10^{-8}	1.34×10^{-3}	1.32×10^{-3}	1.40×10^{-3}		–1.2	4.5
11	4	M1	114.71	1.85×10^{4}	1.83×10^{-7}	5.19×10^{-3}	5.25×10^{-3}	5.28×10^{-3}		1.3	1.8
11	5	E2	132.97	2.08×10^{5}	2.76×10^{-6}	3.87×10^{-2}	3.89×10^{-2}	3.84×10^{-2}	0.4	0.7	–0.7
11	6	E2	135.68	3.18×10^{4}	4.39×10^{-7}	6.54×10^{-3}	6.58×10^{-3}		–1.8	0.6	
11	6	M1	135.68	2.75×10^{6}	3.80×10^{-5}	1.27×10^{0}	1.28×10^{0}	1.28×10^{0}		0.0	0.0
11	7	E2	144.30	7.56×10^{4}	1.18×10^{-6}	2.11×10^{-2}	2.13×10^{-2}		0.0	0.7	
11	7	M1	144.30	2.02×10^{6}	3.15×10^{-5}	1.12×10^{0}	1.13×10^{0}	1.13×10^{0}		0.2	0.1
11	8	E2	172.70	4.52×10^{3}	1.01×10^{-7}	3.10×10^{-3}	3.22×10^{-3}		–1.4	4.0	
11	8	M1	172.70	1.68×10^{6}	3.76×10^{-5}	1.61×10^{0}	1.64×10^{0}	1.61×10^{0}		2.0	–0.1
11	9	M1	628.97	3.35×10^{3}	9.92×10^{-7}	1.54×10^{-1}	1.54×10^{-1}	1.54×10^{-1}		–0.2	0.0

Table 4. (*Continued*).

Upper	Lower	Type	λ	A	gf	S	S_{15}	S_{16}	δS	ΔS_{15}	ΔS_{16}
12	0	E3	46.139	8.60×10^{2}	1.92×10^{-9}	8.52×10^{-3}		8.51×10^{-3}	–0.0		–0.1
12	2	E2	107.83	1.70×10^{4}	2.08×10^{-7}	1.55×10^{-3}	1.61×10^{-3}	1.56×10^{-3}	–3.5	3.6	0.3
12	3	M1	110.81	5.40×10^{3}	6.96×10^{-8}	1.91×10^{-3}	1.91×10^{-3}	1.98×10^{-3}		–0.2	4.0
12	4	E2	111.93	1.72×10^{2}	2.26×10^{-9}	1.89×10^{-5}	2.00×10^{-5}		15	6.0	
12	4	M1	111.93	3.52×10^{3}	4.63×10^{-8}	1.28×10^{-3}	1.30×10^{-3}	1.30×10^{-3}		1.7	1.7
12	5	E2	129.25	9.26×10^{4}	1.62×10^{-6}	2.09×10^{-2}	2.10×10^{-2}		–0.6	0.7	
12	5	M1	129.25	4.82×10^{6}	8.45×10^{-5}	2.70×10^{0}	2.70×10^{0}	2.70×10^{0}		–0.0	–0.1
12	6	E2	131.81	9.36×10^{4}	1.71×10^{-6}	2.33×10^{-2}	2.34×10^{-2}		0.3	0.6	
12	6	M1	131.81	5.93×10^{5}	1.08×10^{-5}	3.53×10^{-1}	3.53×10^{-1}	3.52×10^{-1}		0.0	–0.1
12	7	E2	139.93	7.94×10^{4}	1.63×10^{-6}	2.66×10^{-2}	2.68×10^{-2}		0.8	0.7	
12	7	M1	139.93	1.87×10^{6}	3.85×10^{-5}	1.33×10^{0}	1.33×10^{0}	1.33×10^{0}		0.1	–0.1
12	8	E2	166.48	2.13×10^{4}	6.19×10^{-7}	1.70×10^{-2}	1.70×10^{-2}	1.69×10^{-2}	2.7	0.1	–0.7
12	9	E2	553.63	4.15×10^{1}	1.33×10^{-8}	1.35×10^{-2}	1.36×10^{-2}		–3.8	0.5	
12	9	M1	553.63	5.80×10^{4}	1.86×10^{-5}	2.55×10^{0}	2.55×10^{0}	2.55×10^{0}		–0.1	–0.1

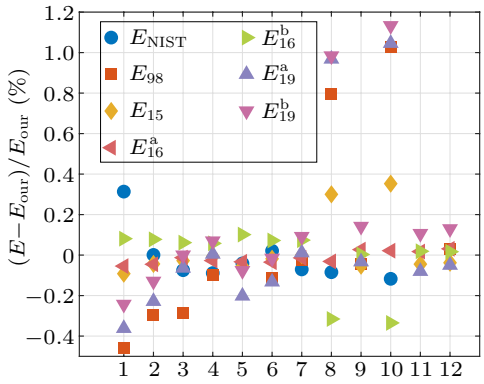


Fig. 3. Relative differences (%) of excited energies (relative to the ground state $4p^6$) between different theoretical and experimental works and our computations (TP+SE2) with the key of energy levels (as shown in Table 3), $E_{\rm NIST}$[70] ($^3F^o_4$ has been adjusted according to 774.8 Å); E_{98};[71] E_{15};[38] $E^{\rm a}_{16}$ [39] (MCDHF); $E^{\rm b}_{16}$ [39] (RMBPT); $E^{\rm a}_{19}$ [41] (GRASP); $E^{\rm b}_{19}$ [41] (FAC).

The following comparisons serve as supplements to the convergence of our calculations. In Table 3, we present excited energies (relative to the ground state $4p^6$) from our TP+SE2 model for the $4p^6$ and $4p^54d$, along with the previous theoretical and measured data. In Fig. 3, we graphically depict the deviations between our results and those of other studies, as detailed in Table 3. Our results exhibit an admirable agreement with the NIST-compiled data,[70] remaining within 0.12%, except for the first excited state $^3P^o_0$ (0.3%). It is noteworthy that at $^3D^o_1$ and $^1P^o_1$, our data exhibit larger relative deviations compared to those of Fournier,[71] Gaigalas *et al.*,[38] and Sharma *et al.*,[41] perhaps resulting from our inclusion of core orbitals (especially 3p, since ours closely match Guo *et al.*[39]) electron correlations. Table 4 provides the E1, M1, E2, M2, and E3 transition parameters among the energy levels outlined in Table 3 (only transitions contributing more than 5×10^{-6} to the lifetime were included). Table 4 illustrated that, except for some weak lines, the relative deviations of line strengths (in length-velocity form) are in the teens percentage-wise, while the rest are within 10%. The line strength under the length gauge[72] $((S-S_{\rm our})/S_{\rm our})$, our results differ by less than 5% from those of Guo *et al.*,[39] and are generally within 8% (expect for $^1P^o_1-{}^1D^o_2$: 19%, weak line) compared to Gaigalas *et al.*[38] In comparison with E1 provided by Sharma *et al.*,[41] the relative deviation ($\lambda_{\rm exp}$ (in unit Å): %) are 80.64:6.1, 63.883:13, and 46.67:27.

4. Conclusions

Adopting the improved calculation model in the present work, by including CC, progressive Breit and SE, it shows that the discrepancy in the wavelength of the $^3F^o_4-{}^3F^o_3$ transition persists −2.8% relative to the previously assigned value 799.23 Å for W^{38+}, while the other spectral lines are within a few tenths of a percent. By anchoring this assignment to the experimental data from W^{39+} spectral line at 774.8 Å, the discrepancy reduces to a mere 0.3%. The experimental data for both spectral lines originates from a single experiment[37] where the two ionic states W^{38+} and W^{39+} are mixed. It is beneficial to conduct additional collision radiation simulations for various ionization states based on high-precision calculations.

In our calculations, electron correlation involved deeper core orbitals (2p) along with higher active orbitals (VV: $n=8$; CV, CC: $n=6,7$), with the number of CSFs associated to $^3F^o_3$ and $^3F^o_4$ being 3 809 748 and 4 021 215, respectively. Inclusion of CC leads to an electron correlation imbalance, as evidenced by changes in both absolute energy and radial electron density distribution of both odd and even parities. We addressed this issue by considering excitation of partial (3p, 3d) core orbitals to $n=7$ and MR. Considering CC and MR, the adjustments to excited energy and electron density are smaller than those from CV and SR, but they did affect the absolute energy of the odd and even parity levels. In this paper, the frequency-dependent correction from TP can reach up to −40% to 2% for Breit interaction, but the various SE methods yield results that are in close agreement, suggesting that no single method exhibits a decisive advantage. These physical effects can serve as a reference for calculations of systems similar to W^{38+}.

We have presented the energy levels (Table 3) and transition parameters (Table 4) for all levels of the $4p^6$ and $4p^5 4d$ of W^{38+} for cross-validated with other relevant data. Since $^3F^o_4$–$^3F^o_3$ is a transition between fine structures, the relative deviation between our calculated result and the measured value remains larger than the experimental uncertainty, which may be attributed to several limitations inherent to our methodology: (i) SCF iterations exclude Breit and QED, and focus solely on optimizing the CSFs of VV layer by layer. (ii) Frequency-dependent contributions are only accounted for spectroscopic orbitals (1s, 2s, 2p, 3s, 3p, 3d, 4s, 4p, 4d, 4f), for other orbitals, we still utilize the low-frequency approximation. (iii) We do not consider higher-order QED. In light of these factors, it would be valuable to obtain higher-resolution experimental measurements – not only for refining the modeling and accurately identifying the $^3F^o_4$–$^3F^o_3$ line, but also for providing a solid benchmark for further theoretical investigations.

Acknowledgements

Project supported by the Science Challenge Project of China Academy of Engineering Physics (CAEP) (Grant No. TZ2018005) and the National Natural Science Foundation of China (Grant Nos. 12474277, 12374259, 12104095, 12074081, and 12074082).

References

[1] Neu R, Dux R, Kallenbach A, Pütterich T, Balden M, Fuchs J, Herrmann A, Maggi C, O'Mullane M, Pugno R, Radivojevic I, Rohde V, Sips A, Suttrop W, Whiteford A and the ASDEX Upgrade Team 2005 *Nuclear Fusion* **45** 209
[2] Wurmshuber M, Doppermann S, Wurster S and Kiener D 2019 *IOP Conference Series: Materials Science and Engineering* **580** 012051
[3] Sizyuk V and Hassanein A 2022 *Sci. Rep.* **12** 4698
[4] Zhu X L, Ke Z H, Cheng L, Zhang P, Yuan Y, Cao X Z and Lu G H 2024 *Nuclear Materials and Energy* **38** 101620
[5] Schmuck K, Burtscher M, Alfreider M and Kiener D 2024 *Materials Design* **247** 113433
[6] Radtke R, Biedermann C, Schwob J L, Mandelbaum P and Doron R 2001 *Phys. Rev. A* **64** 012720
[7] Utter S B, Beiersdorfer P and Trabert E 2002 *Canadian Journal of Physics* **80** 1503
[8] Nakano T, Asakura N, Kubo H, Yanagibayashi J and Ueda Y 2009 *Nuclear Fusion* **49** 115024
[9] Neu R L, Brezinsek S, Beurskens M, Bobkov V, Vries P, Giroud C, Joffrin E, Kallenbach A, Matthews G F, Mayoral M L, Pautasso G, Pütterich T, Ryter F, Schweinzer J, Team A U and Contributors J E 2014 *IEEE Trans. Plasma Sci.* **42** 552
[10] Herrmann A, Zammuto I, Balden M, Greuner H, Jaksic N, Kallenbach A, Li M, Neu R and Rohde V 2017 *Nuclear Materials and Energy* **12** 205
[11] Unterberg E A, Abrams T, Bykov I, Donovan D C, Duran J D, Elder J D, Guo H Y, Hollmann E M, Lasnier C J, Leonard A W, Moser A L, Nichols J H, Nygren R E, Rudakov D L, Stangeby P C, Thomas D M, Victor B S, Watkins J G, Wampler W R, Zach M P, Allen S L, Barton J L, Baylor L R, Boedo J A, Briesemeister A R, Buchenauer D A, Coburn J D, Chrobak C P, Ding R, Ennis D A, Grierson B A, Hinson E T, Johnson C A, McLean A G, Petrie T W, Schmitz O, Shiraki D, Wang H Q, Wilcox R S and Zamperini S 2019 *Nuclear Fusion* **60** 016028
[12] Zito A, Wischmeier M, Kappatou A, Kallenbach A, Sciortino F, Rohde V, Schmid K, Hinson E T, Schmitz O, Cavedon M, McDermott R M, Dux R, Griener M and Stroth U 2023 *Nuclear Fusion* **63** 096027
[13] Jin Y Z, Wang H, Liu X, Lian Y Y, Feng F, Wang J B, Chai Z J, Song J P and Duan X R 2023 *Nuclear Materials and Energy* **36** 101502
[14] Neu R, Fournier K B, Schlogl D and Rice J 1997 *J. Phys. B: At., Mol. Opt. Phys.* **30** 5057
[15] Pütterich T, Neu R, Biedermann C, Radtke R and Upgrade T A 2005 *J. Phys. B: At., Mol. Opt. Phys.* **38** 3071
[16] Morita S, Dong C F, Kato D, Liu Y, Zhang L, Cui Z Y, Goto M, Kawamoto Y, Murakami I and Oishi T 2019 *J. Phys.: Conf. Ser.* **1289** 012005
[17] Xu Z, Zhang L, Cheng Y X, Morita S, Li L, Zhang W M, Zhang F L, Zhao Z H, Zhou T F, Wu Z W, Lin X D, Gao X, Ding X B, Yang Y and Liu H Q 2021 *Nucl. Instrum. Methods Phys. Res. Sec. A: Accelerators, Spectrometers, Detectors and Associated Equipment* **1010** 165545
[18] Boumendjel M Y, Desgranges C, Guirlet R and Peyrusse O 2023 *Phys. Plasmas* **30** 093302
[19] Lei L R, Ding X B, Wu C Q, Zhang D H, Zhang L, Zhang F L, Yao K, Yang Y, Fu Y Q and Dong C Z 2024 *New J. Phys.* **26** 053001
[20] Kallenbach A, Neu R, Dux R, Fahrbach H U, Fuchs J C, Giannone L, Gruber O, Herrmann A, Lang P T, Lipschultz B, Maggi C F, Neuhauser J, Philipps V, Pütterich T, Rohde V, Roth J, Sergienko G, Sips A and Upgrade T A 2005 *Plasma Physics and Controlled Fusion* **47** B207
[21] Pütterich T, Neu R, Dux R, Whiteford A D, O'Mullane M G and the ASDEX Upgrade Team 2008 *Plasma Physics and Controlled Fusion* **50** 085016
[22] Hollmann E M, Commaux N, Shiraki D, Alexander N, Bykov I, Moser A L, Thomas D and Victor B S 2017 *Rev. Sci. Instrum.* **88** 103501
[23] Rzadkiewicz J, Yang Y, Koziol K, O'Mullane M G, Patel A, Xiao J, Yao K, Shen Y, Lu D, Hutton R, Zou Y and Contributors J 2018 *Phys. Rev. A* **97** 052501
[24] Murakami I, Kato D, Oishi T, Goto M, Kawamoto Y, Suzuki C, Sakaue H A and Morita S 2021 *Nuclear Materials and Energy* **26** 100923
[25] Zhang C Y, Wang K, Si R, Li J Q, Song C X, Wu S J, Yan B and Chen C 2023 *Chin. Phys. B* **32** 113102
[26] Ralchenko Y, Draganić I N, Osin D, Gillaspy J D and Reader J 2011 *Phys. Rev. A* **83** 032517
[27] Li J G, Jönsson P, Godefroid M, Dong C Z and Gaigalas G 2012 *Phys. Rev. A* **86** 052523
[28] Tremblay P E, Fontaine G, Fusillo N P G, Dunlap B H, Gänicke B T, Hollands M A, Hermes J J, Marsh T R, Cukanovaite E and Cunningham T 2019 *Nature* **565** 202
[29] Hu S X, Karasiev V V, Recoules V, Nilson P M, Brouwer N and Torrent M 2020 *Nat. Commun.* **11** 1989
[30] Blundell S A, Johnson W R and Sapirstein J 1990 *Phys. Rev. Lett.* **65** 1411
[31] Schiller S 2007 *Phys. Rev. Lett.* **98** 180801
[32] Bieroń J, Gaigalas G, Gaidamauskas E, Fritzsche S, Indelicato P and Jönsson P 2009 *Phys. Rev. A* **80** 012513
[33] Berengut J C, Dzuba V A and Flambaum V V 2010 *Phys. Rev. Lett.* **105** 120801
[34] Tsai Y D, Eby J and Safronova M S 2022 *Nature Astronomy* **7** 113
[35] Zhang X, Banerjee A, Leyser M, Perez G, Schiller S, Budker D and Antypas D 2023 *Phys. Rev. Lett.* **130** 251002
[36] Göttel A S, Ejlli A, Karan K, Vermeulen S M, Aiello L, Raymond V and Grote H 2024 *Phys. Rev. Lett.* **133** 101001
[37] Radtke R, Biedermann C, Fumann G, Schwob J L, Mandelbaum P and Doron R 2007 *Atomic and Plasma-Material Interaction Data for Fusion* **13** 45
[38] Gaigalas G, Rynkun P and Froese Fischer C 2015 *Phys. Rev. A* **91** 022509
[39] Guo X L, Grumer J, Brage T, Si R, Chen C Y, Jönsson P, Wang K, Yan J, Hutton R and Zou Y M 2016 *J. Phys. B: Atom., Mol. Opt. Phys.* **49** 135003
[40] Lindgren I 1974 *J. Phys. B: Atom. Mol. Phys.* **7** 2441
[41] Sharma R, Goyal A and Mohan M 2019 *Journal of Electron Spectroscopy and Related Phenomena* **234** 47
[42] Dyall K G, Grant I P, Johnson C T, Parpia F A and Plummer E P 1989 *Comput. Phys. Commun.* **55** 425
[43] Gu M F 2008 *Canadian Journal of Physics* **86** 675
[44] Beier T, Mohr P J, Persson H and Soff G 1998 *Phys. Rev. A* **58** 954
[45] Le Bigot E O, Indelicato P and Mohr P J 2001 *Phys. Rev. A* **64** 052508
[46] Welton T A 1948 *Phys. Rev.* **74** 1157
[47] Shabaev V M, Tupitsyn I I and Yerokhin V A 2013 *Phys. Rev. A* **88** 012513
[48] Malyshev A V, Glazov D A, Shabaev V M, Tupitsyn I I, Yerokhin V A and Zaytsev V A 2022 *Phys. Rev. A* **106** 012806

[49] Grant I P, McKenzie B J, Norrington P H, Mayers D F and Pyper N C 1980 *Comput. Phys. Commun.* **21** 207

[50] Jönsson P, Gaigalas G, Froese Fischer C, Bieroń J, Grant I P, Brage T, Ekman J, Godefroid M, Grumer J, Li J G and Li W X 2023 *Atoms* **11** 68

[51] Zhang C Y, Wang K, Godefroid M, Jönsson P, Si R and Chen C Y 2020 *Phys. Rev. A* **101** 032509

[52] Zhang C Y, Wang K, Godefroid M, Jönsson P, Si R and Chen C Y 2021 *Journal of Quantitative Spectroscopy and Radiative Transfer* **269** 107650

[53] Guo X L, Huang M, Yan J, Li S, Wang K, Si R and Chen C Y 2015 *Chin. Phys. B* **25** 013101

[54] Froese Fischer C 2014 *Atoms* **2** 1

[55] Froese Fischer C, Brage T and Jönsson P 2022 *Computational Atomic Structure: An MCHF Approach* (New York: Routledge) pp. 171–177

[56] Jönsson P, Godefroid M, Gaigalas G, Ekman J, Grumer J, Li W X, Li J G, Brage T, Grant I P, Bieroń J and Froese Fischer C 2022 *Atoms* **11** 7

[57] Mittleman Marvin H 1972 *Phys. Rev. A* **5** 2395

[58] Indelicato P 2019 *J. Phys. B: Atom., Mol. Opt. Phys.* **52** 232001

[59] Grant I P and Pyper N C 1976 *J. Phys. B: Atom. Mol. Phys.* **9** 761

[60] Uehling E A 1935 *Phys. Rev.* **48** 55

[61] Wichmann E H and Kroll N M 1956 *Phys. Rev.* **101** 843

[62] Fullerton L W and Rinker G A 1976 *Phys. Rev. A* **13** 1283

[63] Beier T, Plunien G, Greiner M and Soff G 1997 *J. Phys. B: Atom., Mol. Opt. Phys.* **30** 2761

[64] Mohr P J 1983 *Atomic Data and Nuclear Data Tables* **29** 453

[65] Klarsfeld S and Maquet A 1973 *Phys. Lett. B* **43** 201

[66] Schiffmann S, Li J G, Ekman J, Gaigalas G, Godefroid M, Jönsson P and Bieroń J 2022 *Comput. Phys. Commun.* **278** 108403

[67] Gaigalas G, Froese Fischer C, Rynkun P and Jönsson P 2017 *Atoms* **5** 5

[68] Guo X L, Li M C, Si R, He X D, Wang K, Dai Z T, Liu Y M, Zhang H J and Chen C Y 2017 *J. Phys. B: Atom., Mol. Opt. Phys.* **51** 015002

[69] Wang K, Zhang C Y, Si R, Li S, Chen Z B, Zhao X H, Chen C Y and Yan J 2018 *Atomic Data and Nuclear Data Tables* **123–124** 114

[70] Kramida A, Yu Ralchenko, Reader J and and NIST ASD Team 2022 NIST Atomic Spectra Database (Ver. 5.10), [Online]. Available: `https://physics.nist.gov/asd` [2023, December 4]. National Institute of Standards and Technology, Gaithersburg, MD

[71] Fournier K B 1998 *Atomic Data and Nuclear Data Tables* **68** 1

[72] Shi B L, Q Y, Li X F, Deng B L, Jiang G and Dou X L 2022 *Chin. Phys. B* **31** 053102